inorganics

MDPI

Article

Complexation of Boron and Aluminum with a Bidentate Hydroxy-BN-naphthalene Ligand

Yannik Appiarius [1,2], Pim Puylaert [3], Julius Werthschütz [4], Tim Neudecker [2,4,5] and Anne Staubitz [1,2,*]

[1] University of Bremen, Institute for Organic and Analytical Chemistry, 28359 Bremen, Germany; yappiarius@uni-bremen.de
[2] University of Bremen, MAPEX Center for Materials and Processes, 28359 Bremen, Germany; neudecker@uni-bremen.de
[3] University of Bremen, Institute for Inorganic Chemistry and Crystallography, 28359 Bremen, Germany; puylaert@uni-bremen.de
[4] University of Bremen, Institute for Physical and Theoretical Chemistry, 28359 Bremen, Germany; jwerthsc@uni-bremen.de
[5] University of Bremen, Bremen Center for Computational Materials Science, 28359 Bremen, Germany
* Correspondence: staubitz@uni-bremen.de

Abstract: The isoelectronic relationship of 1,2-azaborinine (B=N structural motif) and benzene (C=C) is well documented. Upon deprotonation of the former, the anionic 1,2-azaboratabenzene is obtained, which is isosteric with pyridine (C=N) and has a similar capability as an aromatic *N*-donor. We present the complexation of boron and aluminum precursors with a κ^2-*N*,*O*-donating 8-hydroxy-BN-naphthalene ligand (**H_2(BQ)**, **1**). Six chelate complexes with 1:1 and 2:1 stoichiometries were isolated and characterized by X-ray diffraction analysis and NMR spectroscopy. Comparing the isosteric dimethylaluminum complexes of **H_2(BQ)** and an 8-hydroxyquinoline (**HQ'**, **2**) as a reference allowed us to quantify the influence of a formal substitution of carbon by boron on the structure and the electronic properties: While the structural parameters of the ligands were similar, the electropositive boron atom affected the electron density distributions within the complexes substantially. As the consequence, the Al–N bond was significantly shortened, and the aluminum atom showed a different coordination geometry than in the quinoline analog. Moreover, strong hypsochromic shifts of both the absorption and the emission were observed. The results highlight that the differences between CN and BN polyaromatic complexes are more distinct than between equally charged BN and CC congeners.

Keywords: 1,2-azaborinines; boron–nitrogen chemistry; BN chemistry; polycyclic aromatic hydrocarbons; heteroaromatics; aluminum; boron; bidentate ligands; 8-hydroxyquinoline

Citation: Appiarius, Y.; Puylaert, P.; Werthschütz, J.; Neudecker, T.; Staubitz, A. Complexation of Boron and Aluminum with a Bidentate Hydroxy-BN-naphthalene Ligand. *Inorganics* **2023**, *11*, 295. https://doi.org/10.3390/inorganics11070295

Academic Editors: Jean-François Halet and Gilles Alcaraz

Received: 21 June 2023
Revised: 7 July 2023
Accepted: 10 July 2023
Published: 12 July 2023

1. Introduction

Six-membered heterocycles comprising neighboring boron and nitrogen atoms have attracted significant attention because taken together, BN and CC groups share the same electron configurations (Figure 1, top) [1,2]. As a result, 1,2-azaborinine not only resembles benzene geometrically, but the increased π-character of a B=N bond also gives rise to a substantial degree of aromaticity [3–5]. However, the significant divergence in polarity induces distinct reactivities of the individual ring atoms [6] and strongly altered optical properties [7,8]. The elucidation of the influence of a formal BN substitution has been the subject of numerous studies, also including polycyclic derivatives like BN-naphthalenes [9–12].

Different from all-carbon aromatics, the NH-acidity in 1,2-azaborinines ($pK_a \approx$ 24–26) [6,13] facilitates their selective deprotonation to afford 1,2-azaboratabenzenes. It has been demonstrated that these anionic monocycles may serve as η^1-donating ligands for the complexation of electrophiles or metals (Be, B, Al, Ga, Si, Sn, Zr), establishing stable covalent bonds via the nitrogen atoms [14,15]. More recently, deprotonated pyridyl-substituted

BN aromatics have been used for the chelation of iridium(III) ions [16] or a dimesitylboron unit [17] (Figure 1, bottom left).

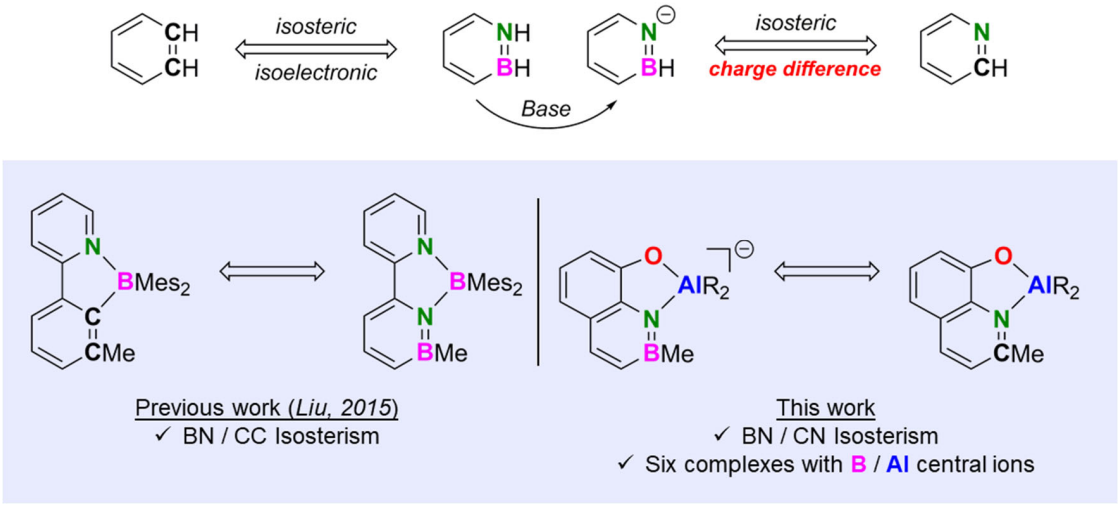

Figure 1. (**Top**): Structural relationships of benzene, (de-)protonated 1,2-azaborinine and pyridine. (**Bottom**): Previous work (left) and concept of this work (right). Reprinted (adapted) with permission from [17]. Copyright (2015) American Chemical Society.

The resulting uncharged κ^2-*N*,*N* complexes showed particularly altered optical properties, compared to their CC counterparts, which highlights their application potential for light-emitting devices. While the electron density distributions and basicities (pKa of pyridinium ≈ 5) [18] differ significantly, 1,2-azaboratabenzene can be treated as an anionic congener of pyridine regarding the atom placements and its nucleophilic nitrogen atom [19]. To our knowledge, the isosteric relationship between deprotonated 1,2-azaborinines and pyridines has not been investigated, particularly with respect to their use as bidentate ligands for the complexation of main group elements.

Herein, we describe the synthesis of a 2-methyl-8-hydroxy-BN-naphthalene (**H_2(BQ)**, **1**), which becomes suitable as a κ^2-*N*,*O* donor upon deprotonation. The BN ligand was used for the chelation of aluminum- and boron-precursors, affording six complexes with 1:1 (**M[R_2E(BQ)]**; M = Li, Na; R = alkyl, Ph; E = B, Al) and 2:1 (**M[E(BQ)$_2$]**) ligand to central ion (E) stoichiometries. The anionic nature of the complexes complies with the tendency of Lewis acidic boron and aluminum to form tetravalent structures.

BN ligand **1** is structurally similar to 8-hydroxyquinoline (**HQ**), which is a potent ligand for the one-to-threefold chelation of group 13 elements [20–24]. The ligand and its complexes have various applications, for instance in the selective detection and separation of metal ions and the therapeutic use as chelator (**HQ**), as well as for their use as emitting materials in organic light emitting diodes (OLED) (**AlQ_3**). Intending to probe the influence of a formal BN vs. CN-substitution while leaving the geometry mostly unaffected, we used the exact CN counterpart 2-methyl-8-hydroxyquinoline (**HQ′**, **2**) to synthesize **[Me_2Al(Q′)]$_2$** (**3**). This enabled the experimental and theoretical comparison with **Li[Me_2Al(BQ)]** (**4**) with respect to the molecular structures as well as optical and electronic properties. The alkylaluminum complexes were chosen representatively because methyl groups do not tend to play a major electronic and steric role in the ligand-to-metal bond formation, which was one of our key interests.

2. Results and Discussion

2.1. Syntheses

The synthesis of the BN ligand **1** was initiated by a Suzuki–Miyaura cross-coupling reaction of 2-bromo-6-methoxyaniline (**5**) with potassium vinyltrifluoroborate (Scheme 1). The resulting 2-methoxy-6-vinylaniline (**6**) was then converted to 8-methoxy-BN-naphthalene **7** using a

reported annulation/aromatization sequence in cyclopentyl methyl ether (CPME) and toluene as the solvents [11]. Eventually, **1** was obtained via boron-tribromide-mediated ether cleavage in an overall yield of 29% over three steps.

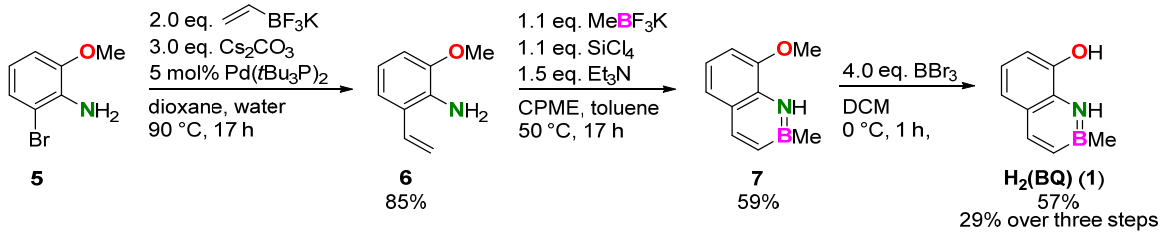

Scheme 1. Preparation of ligand **1** by cross coupling, BN bond formation and ether cleavage.

The complexation reactions involving the BN ligand were conducted under strictly inert conditions in mixtures of dry 1,4-dioxane and dry THF-d_8. If required, **H_2(BQ)** was deprotonated in situ with 2.50 equiv. of lithium bis(trimethylsilyl)amide (LHMDS) to form **Li_2(BQ)** (**8**, Scheme 2). Subsequently, the respective boron or aluminum reagent was added and, if necessary, the reaction was heated until a quantitative conversion was found by ^{1}H nuclear magnetic resonance (NMR) spectroscopy.

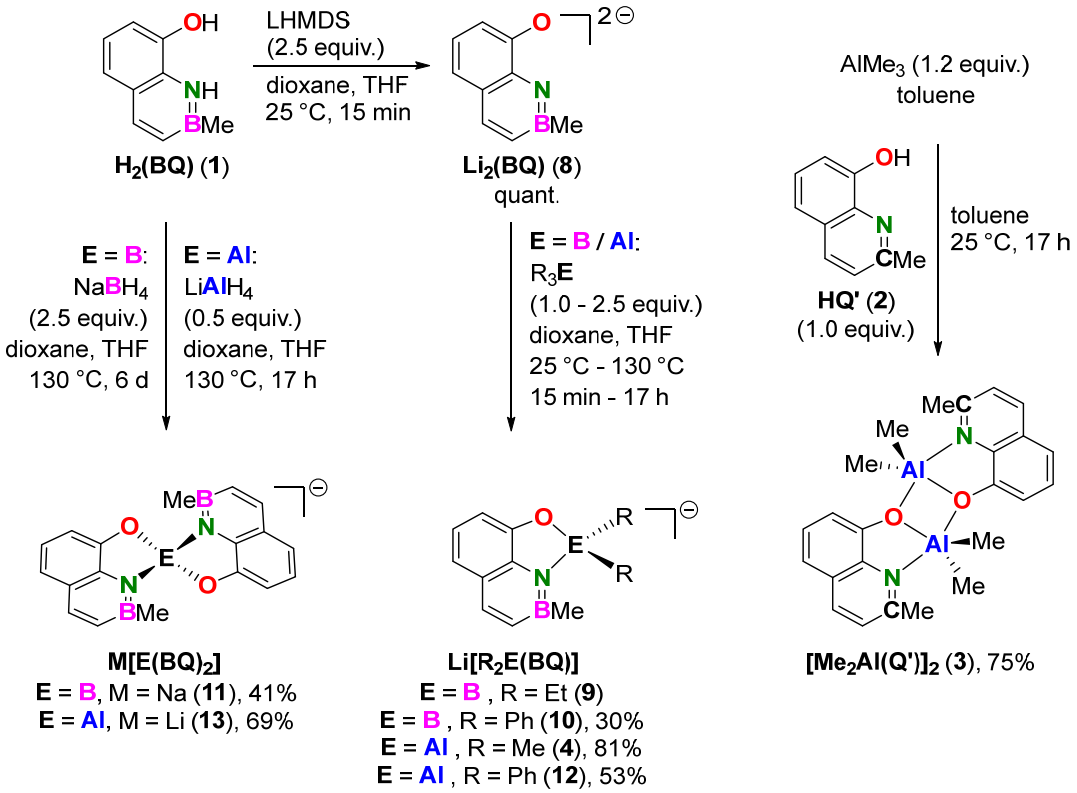

Scheme 2. Overview of the complexation reactions of **H_2(BQ)** and **HQ′**. Counter cations omitted in the molecular structures.

All complexation reactions involving the BN naphthalene ligand and reagents of the type ER_3 were performed starting from **7**. This allowed us to synthesize the 1:1 complexes **Li[Et_2B(BQ)]** (**9**), **Li[Ph_2B(BQ)]** (**10**), **Li[Me_2Al(BQ)]** (**4**) and **Li[Ph_2Al(BQ)]** (**12**) (Table 1). However, the use of the respective boron or aluminum reagents (BEt_3, BPh_3, $AlMe_3$ and $AlPh_3$) in equimolar amounts led to the preferred formation of unreactive, tetravalent species of the type $LiBR_4$. These species likely form between ER_3 and alkyl-/phenyl groups that are cleaved during complexation. Only in the case of **12**, an equimolar amount of $AlPh_3$

was expedient. Therefore, we used a 2.5-fold excess of the reagents for the syntheses of **9**, **10** and **4**, which ensured quantitative conversions of the ligands and higher reaction rates. Notwithstanding, the approach towards **9** revealed the presence of inseparable $LiBEt_4$ ($\delta^{11}B$ = –16.5 ppm) [25] after the reaction. We attribute this to the high Lewis acidity of BEt_3. While the reactions involving AlR_3 immediately revealed a complete conversion, BR_3 reagents reacted much more slowly and required heating to 130 °C for 17 h.

Table 1. Reaction conditions and isolated yields.

Entry	Reagent (Equiv.)	Ligand	T	t	Product (#) [a]	Yield
1	BEt_3 (2.50)	**8**	130 °C	17 h	**Li[Et_2B(BQ)]** (**9**)	[b]
2	BPh_3 (2.50)	**8**	130 °C	17 h	**Li[Ph_2B(BQ)]** (**10**)	30%
3	$NaBH_4$ (2.50)	**1**	130 °C	6 d	**Na[B(BQ)$_2$]** (**11**)	41%
4	$AlMe_3$ (2.50)	**8**	25 °C	15 min	**Li[Me_2Al(BQ)]** (**4**)	81%
5	$AlPh_3$ (1.00)	**8**	25 °C	15 min	**Li[Ph_2Al(BQ)]** (**12**)	53%
6	$LiAlH_4$ (0.50)	**1**	130 °C	17 h	**Li[Al(BQ)$_2$]** (**13**)	69%
7	$AlMe_3$ (1.20)	**2**	25 °C	17 h	**[Me_2Al(Q')]$_2$** (**3**)	75%

[a] Complexed solvent molecules omitted. [b] Yield not determinable due to a contamination with $LiBEt_4$.

In contrast to this, complex metal hydrides $NaBH_4$ and $LiAlH_4$ were sufficiently basic to deprotonate **1** in situ, so that the initial treatment with LHMDS was unnecessary. However, the reaction with $NaBH_4$ was sluggish and required a reaction time of 6 d at 130 °C. Interestingly, the use of an excess of $NaBH_4$ (2.50 equiv.) did not lead to the expected 1:1 complex but to **Na[B(BQ)$_2$]** (**11**), which could not be obtained cleanly when using the required precursor ratio of 2:1. We attribute this to the limited solubility of $NaBH_4$ in dioxane and THF. $LiAlH_4$ was more reactive, allowing to obtain **Li[Al(BQ)$_2$]** (**13**) by the addition of 0.50 equiv. of $LiAlH_4$ and heating the reaction to 130 °C for 17 h.

The isolation of crystalline products was achieved either by crystallization or by washing/extracting the crude products in a glove box, yielding 30% to 81%. As the only complex, **9** remained an oil due to its contamination with $LiBEt_4$.

The complexes revealed similarly shifted signals in the aromatic regions of the ^1H NMR spectra (δ^1H = 7.5–7.8 ppm and 6.2–6.9 ppm). In the $^{11}B\{^1H\}$ NMR spectra, broad signals at $\delta^{11}B$ = 35–40 ppm were found, confirming the small influence of complexation on the aromatic nature of the azaborinines. All structures with complexed boron revealed the presence of secondary resonances at $\delta^{11}B$ = 13.3 (**9**), 10.5 (**10**) and 15.2 (**11**) ppm (see ESI, Section 2), which is comparable with the reported **[Ph_2B(Q)]** ($\delta^{11}B$ = 11.9 ppm) [26].

For the synthesis of the hydroxyquinoline complex **[Me_2Al(Q')]$_2$** (**3**), a slight excess of $AlMe_3$ was dissolved in dry toluene. Subsequently, a solution of **HQ'** was added. The resulting precipitation was filtered, and the product was obtained in 75% yield (Scheme 2).

Due to the highly unsymmetrical environments of the central ions, the complexes of aluminum did not allow to obtain ^{27}Al NMR spectra. However, all structures were unequivocally confirmed by mass spectrometry and X-ray diffraction analysis.

2.2. X-ray Diffraction Analysis

The molecular structures of the complexes of **H_2(BQ)** and **HQ'** with boron (Figure 2 and Table 2) and aluminum (Figure 3 and Table 3) as central ions were obtained by X-ray diffraction analysis. All anionic complexes of the BN ligand crystallized with the respective counterions in close proximity (Li ≈ 1.9 Å, Na ≈ 2.4 Å) to the oxygen atoms and two to three solvent molecules per ligand-central ion complex. Moreover, the central ions showed distorted tetrahedral geometries in all cases.

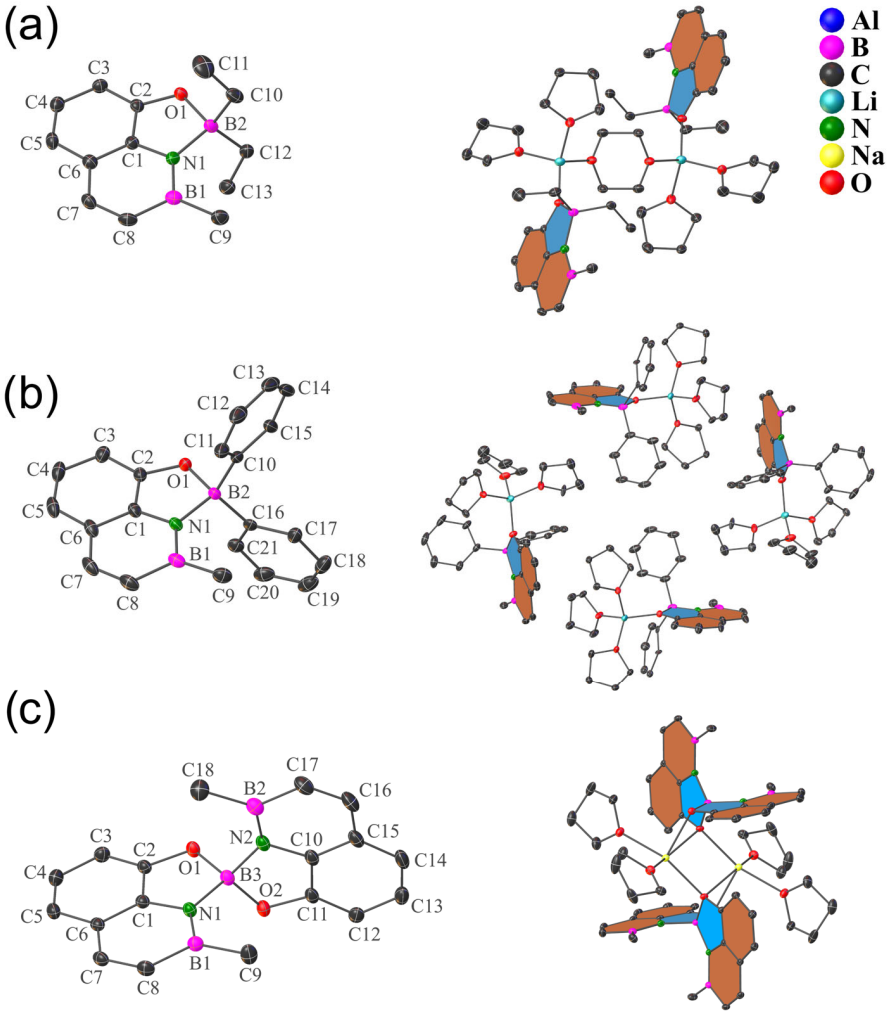

Figure 2. Solid-state structures of complexes **9** (**a**), **10** (**b**) and **11** (**c**). Left: Single complexes with counterions and solvent molecules omitted. Right: Crystal packings. Hydrogen atoms were omitted for clarity.

Table 2. Key crystal structure details of the boron complexes of **H_2(BQ)**.

Entry	Complex Structure	B–O [Å]	B–N [Å]	B–C [Å]	O–M [Å] [a]	V [Å^3] [b]
1	**([Li(THF)$_2$(diox)$_{0.5}$][Et$_2$B(BQ)])$_2$ (9)** [c]	1.590 (4)	1.587 (4)	1.610 (5), 1.616 (4)	1.885 (5)	2.077
2	**[Li(THF)$_3$][Ph$_2$B(BQ)] (10)** [d]	1.573 (2)	1.574 (2)	1.619 (2), 1.621 (2)	1.935 (3)	2.059
3	**([Na(THF)$_2$][B(BQ)$_2$])$_2$ (11)**	1.499 (2), 1.518 (2)	1.593 (2), 1.546 (2)	-	2.3558 (12)	1.797

[a] M = Li/Na. [b] Tetrahedral volume around B. [c] diox = 1,4-dioxane. [d] Structural features given for the non-disordered part.

In contrast, the molecular structure of quinolinolate **3** confirmed the supposed dimerization, which has been reported for similar Al complexes of **HQ** with little steric demand of the alkyl substituents [27]. As a result, the pentacoordinate aluminum atom of **[Me$_2$Al(Q′)]$_2$** adopted a distorted trigonal-bipyramidal coordination geometry, with a relatively large distance to O1′ of the opposite monomer unit (Al–O1′ ≈ 2.01 Å, Figure 3d).

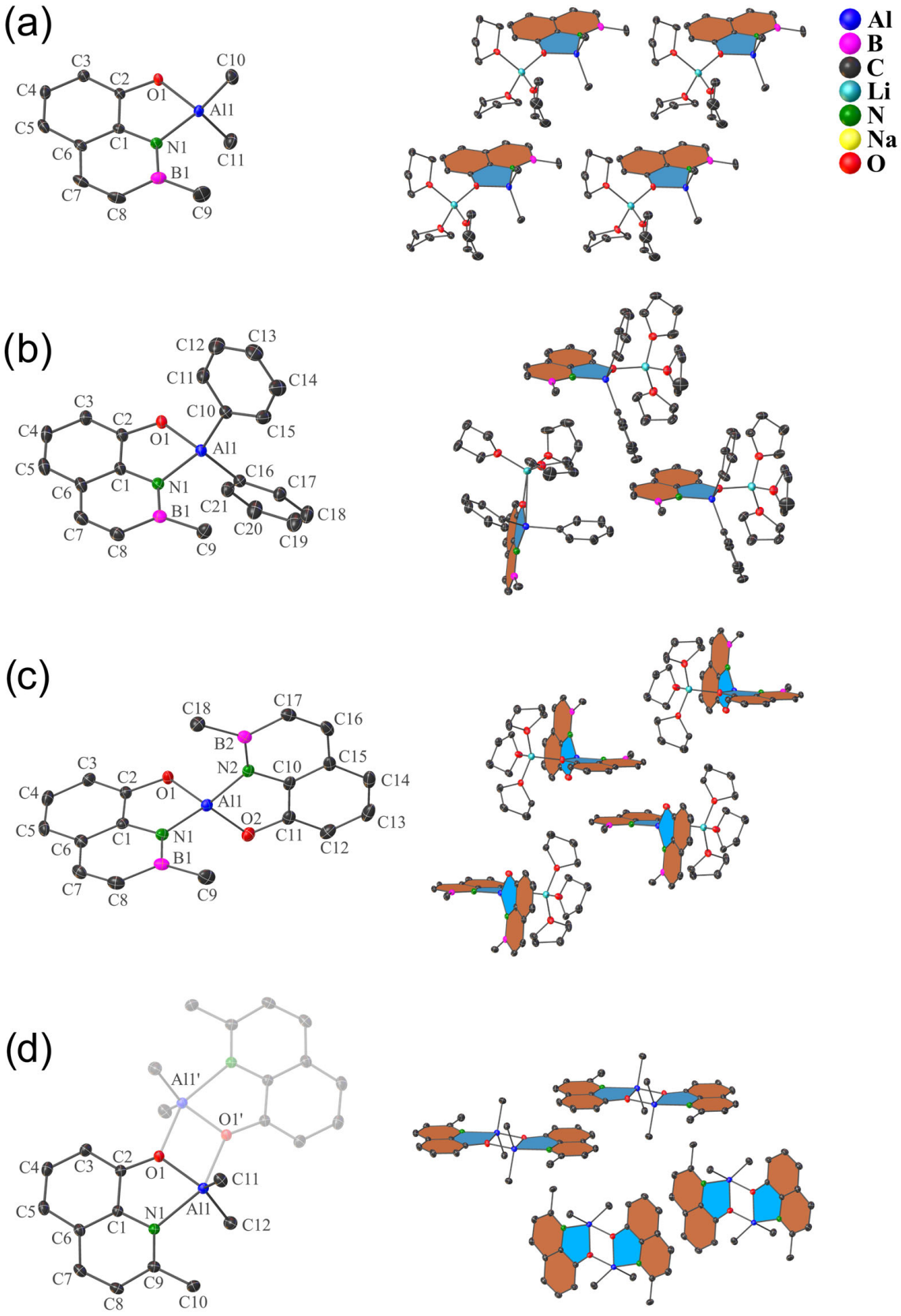

Figure 3. Solid-state structures of complexes **4** (**a**), **12** (**b**), **13** (**c**) and **3** (**d**). Left: Single complexes with counterions and solvent molecules omitted. Right: Crystal packings. Hydrogen atoms were omitted for clarity.

Table 3. Key crystal structure details of the aluminum complexes of **H_2(BQ)** and **HQ′**.

Entry	Complex Structure	Al–O [Å]	Al–N [Å]	Al–C [Å]	O–M [Å] [a]	V [Å^3] [b]
1	**[Li(THF)$_3$] [Me$_2$Al(BQ)]** (**4**)	1.8368 (14)	1.9091 (17)	1.969 (2), 1.974 (2)	1.892 (3)	3.471
2	**[Li(THF)$_3$] [Ph$_2$Al(BQ)]** (**12**)	1.832 (2)	1.890 (3)	1.976 (3), 1.977 (3)	1.916 (6)	3.452
3	**[Li(THF)$_3$] [Al(BQ)$_2$]** (**13**)	1.7741 (14), 1.7879 (15)	1.8565 (17), 1.8570 (17)	-	1.923 (4)	2.876
4	**[Me$_2$Al(Q′)]$_2$** (**3**)	1.8732 (9)	2.1293 (11)	1.9756 (12), 1.9787 (11)	2.0082 (8)	-

[a] M = Li/Na/Al′ of secondary monomer within the dimer. [b] Tetrahedral volume around Al.

With respect to the ligand backbones, low maximum torsion angles ($\varphi < 2.4^\circ$) indicate planarity in all cases. The azaborinine units showed comparable bond lengths, typical of BN-naphthalenes (N1–C1: 1.376–1.392 Å; N1–B1: 1.420–1.427 Å; B1–C8: 1.537–1.545 Å; B1–C9: 1.574–1.591 Å; C2–O1: 1.356–1.380 Å) [10,28].

The formal substitution of boron by a carbon atom in **[Me$_2$Al(Q′)]$_2$** expectedly lowered the bond lengths to its bonding partners (Δ B1/C9–N1 = 0.094 Å, Δ B1/C9–CH_3 = 0.083 Å, Δ B1/C9–CH = 0.127 Å). Little variance was found between the bond lengths of **3** and **4** involving the phenol units and the Al–O/Al–C bonds (Δ C2–O1 = 0.014 Å, Δ Al1–O1 = 0.036 Å, Al1–C = 0.003 Å). As anticipated, the averaged B–O bond lengths were much smaller (average **9**, **10**, **11**: 1.545 Å) than the respective Al–O bond lengths (average **4**, **12**, **13**: 1.808 Å). The same trend was observed for B–N and Al–N (1.575 Å/1.878 Å) as well as B–C and Al–C (1.617 Å/1.974 Å) bonds, involving the central ions.

With respect to hydroxyquinoline complexes with analogous (alkyl/phenyl)$_2$ substitution at boron (B–O ≈ 1.55 Å, B–N ≈ 1.62 Å) [29,30] these bond lengths were in the same range but more compensated in **9** and **10** (both B–O and B–N ≈ 1.58 Å).

The Al–N bond length of **4** (≈1.91 Å) was similar to complexes of pyrrole (≈1.88 Å) [31] and slightly decreased compared to **[*t*Bu$_2$Al(Q)]** (≈1.98 Å), which crystallizes as a monomer for steric reasons [32]. In contrast, this bond length was increased significantly within dimeric **3** (≈2.13 Å). Here, both the more coordinative character of the Al–N bond as well as the axial coordination to the trigonal-bipyramidal aluminum atom induce this elongation, compared to the Al–N σ-bond within azaborinine **4**.

Comparing the complexes of the BN ligand with 1:1 and 2:1 stoichiometries, the E-O and E-N bond lengths were significantly shortened in 2:1 complexes **11** and **13** (Δ ≈ 0.05 Å for E = Al). This was also reflected by the decreased volumes of the tetrahedra around B (≈87% of the averaged volumes of the **Li[R$_2$B(BQ)]** species) and Al (≈83%). The reducing effect of a second quinolinolate ligand around an Al center on the Al–O and Al–N bond lengths has been reported in a theoretical study [33].

With respect to the crystal packings of the boron complexes, **9** has two molecules of THF in the coordination sphere of the lithium ion. Moreover, one molecule of 1,4-dioxane (diox) bridges two of such units via the lithium atoms (Figure 2). **10** crystallized with a lithium counterion, surrounded by three molecules of THF per asymmetric unit. **11** crystallized in dimeric fashion, where two units of the 2:1 complexes are bridged via both of their oxygen atoms and two sodium counterions, forming a four-membered Na_2O_2 ring. Each of the sodium ions is furthermore complexed by two molecules of THF.

All BN complexes with aluminum as central ion crystallized with lithium counterions, surrounded by three molecules of THF per asymmetric unit (Figure 3). The crystal packings of **9** and **10** were dominated by the space-filling tetrahedral [Li(THF)$_3$] units, preventing a close approximation of neighboring ligand units (centroid distances ≈ 7.5 Å). In contrast, the crystal packing of **11** revealed that the BN-naphthalene planes of neighboring molecules were stacked in head-to-tail fashion, with plane-to-plane centroid distances of 3.35 Å. Consequently, **11** was the only investigated complex where π–π stacking played a notable role in the solid-state interactions.

2.3. Theoretical Analysis

The structural and electronic parameters of **Li[Me_2Al(BQ)]** (**4**) and **[Me_2Al(Q′)]$_2$** (**3**) were further analyzed by density functional theory (DFT) [34,35] calculations at the CAM-B3LYP [36]/cc-pVDZ [37] level of theory, as implemented in the Orca 5.0 [38] and Gaussian 16 [39] program packages. In all cases, the absence of imaginary frequencies ensured that the geometry optimizations led to minimum energetic structures.

Anionic **[Me_2Al(BQ)]$^-$** (**14**) and monomeric **[Me_2Al(Q′)]** (**15**) were also included in the theoretical investigation in order to estimate the influence of ion association in **4** and dimerization in **3** on structure and electronics.

The calculated bond lengths were in good agreement with the results from X-ray diffraction analysis for the aromatic bonds within the polycyclic aromatic hydrocarbon (PAH) backbones and the Al–C bonds (Δd < 0.03 Å). Higher deviations were found for the C–O, Al–O and Al–N bonds, strongly depending on the inclusion of counterion and secondary monomer unit into the calculations (Table 4). These results indicate that the actual Al–O/N bonding situations in the BN and CN complexes are best described as intermediates between both calculated forms.

Figure 4 illustrates the charge distributions within quinoline **3** and BN-naphthalene **4**, visualized with Multiwfn [40]. Overall, both complexes resemble each other in terms of the electron-rich phenol rings and the electron-deficient carbon atoms within the nitrogen-containing rings. Moreover, the low charge densities at boron and aluminum are apparent. The electron densities were further analyzed by Natural Bond Orbital (NBO) calculations [41]. With respect to the influence of a boron vs. carbon substitution, the presence of an electropositive boron atom in **4** (natural charge: +0.89, cf. +0.30 for the equivalent C9 of **3**) induced drastically increased negative charges at its bonding partners.

In particular, the nitrogen atom of **4** had a much higher negative charge (–1.09), which was associated with an increased p-orbital occupancy ($2p^{4.70}$) compared with **3** (–0.58, $2p^{4.25}$). On the other hand, the oxygen atoms of both compounds showed comparable natural charges (–1.00 and –0.92) and electron configurations. These results rationalize the experimentally and theoretically obtained similarities in Al–O bond lengths concomitant with fundamentally different Al–N bond properties.

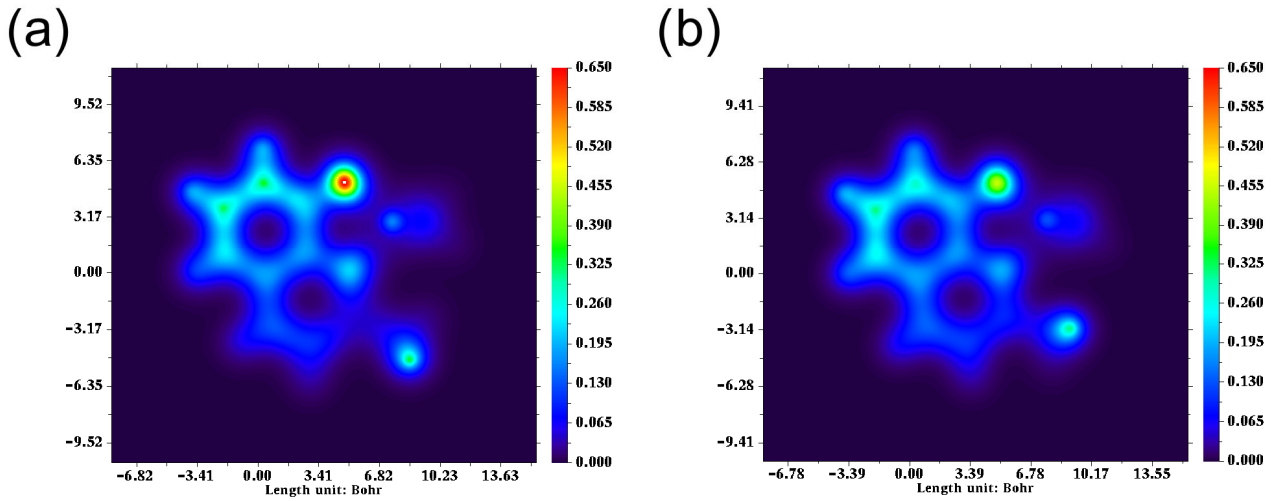

Figure 4. Wavefunction derived electron density distributions within **14** (**a**) and **15** (**b**). Blue = electron-poor, red = electron-rich. Note: Al-CH_3 groups protrude from the polycyclic aromatic hydrocarbon (PAH) plane; thus, their color-codings are not meaningful.

Table 4. Structural and electronic parameters calculated at the CAM-B3LYP/cc-pVDZ level of theory and comparison with results from X-ray diffraction analysis.

	Li[Me_2Al(BQ)] (4)	**[Me_2Al(Q′)]$_2$ (3)**
Bond Lengths [a]/Wiberg Bond Indices (WBI)		
Al1–O1	Calcd. 1.900 Å X-ray: 1.837 Å (Calcd. **14**: 1.846 Å) WBI: 0.33	Calcd. 1.913 Å X-ray: 1.873 Å (Calcd. **15**: 1.838 Å) WBI: 0.25
Al1–N1	Calcd. 1.901 Å X-ray: 1.909 Å (**14**: 1.953 Å) WBI: 0.38	Calcd. 2.220 Å X-ray: 2.129 Å (**15**: 2.058 Å) WBI: 0.19
Al1–O1′	-	Calcd. 2.055 Å X-ray: 2.010 Å WBI: 0.18
Natural Atomic Charges/Electron Configurations [a][b]		
Al1	+1.86/$3s^{0.51}3p^{0.60}$	+1.91/$3s^{0.50}3p^{0.57}$
O1	–1.00/$2s^{1.68}2p^{5.32}$	–0.92/$2s^{1.63}2p^{5.28}$
N1	–1.09/$2s^{1.38}2p^{4.70}$	–0.58/$2s^{1.31}2p^{4.25}$
B1/C9	+0.89 (B1)	+0.30 (C9)
C8	–0.56	–0.27
C9/C10	–1.01 (C9)	–0.68 (C10)
Sum of Donor–Acceptor Orbital Interactions (*E(2)*)[a][b][c]		
LP O→LV Al	143.6 kcal mol^{-1}	201.6 kcal mol^{-1}
LP N→LV Al	127.7 kcal mol^{-1}	73.7 kcal mol^{-1}
LP C→LV Al	459.8 kcal mol^{-1}	442.3 kcal mol^{-1}

[a] Atom numberings as in Figure 3. Averaged values are given for chemically equivalent groups. [b] Contributions of the 3d orbitals (≤0.02) were omitted. [c] Performed by second order perturbation theory analysis of Fock Matrix in Natural Bond Orbital (NBO) basis. *E(2)* = stabilization energies associated with delocalization. LP = lone pair orbital, LV = lone valency orbital. Interactions with Rydberg orbitals were omitted because these energies were negligibly small.

The natural charge of the aluminum ion (≈+1.90) was independent of the nature of the PAH ligand and complies with approximately 1.1 electrons located in the lone valency orbitals at the aluminum atoms, adding up to the ionic charge of Al(III).

Comparing the natures of the B–N and the C–N-bonds, both the σ- and the π-components of the bonds are highly polarized. In azaborinine **4**, 79% of the σ-bond and 86% of the π-bond density are localized at the nitrogen atom, while it is only 62% and 64% in pyridine **3**, complying with the smaller difference of the Natural Atomic Charges between both heteroatoms in this complex (Table 4).

The donor–acceptor characteristics involving the aluminum atoms were further studied by second order perturbation theory. Here, the interactions between occupied Lewis-type NBOs (lone pairs (LP) at N and O of the PAH ligands and C of the Al-CH_3 groups) and vacant non-Lewis type NBOs (lone valencies (LV) at Al) are examined. Such orbital overlaps lead to a deviation from the idealized Lewis-type orbital localizations, which can be quantified by calculating the associated stabilization energy *E(2)*. While these total energies were dominated by the contributions of the methyl groups (LP C→LV Al, *E(2)* ≈ 450 kcal mol^{-1}), LP O/N→LV Al interactions made up ca. 270 kcal mol^{-1} of the total stabilization energies in both cases. However, the LP at the nitrogen atom accounted for a significantly higher share in BN complex **4** (127.7 kcal mol^{-1}) than in CN-analog **3** (73.7 kcal mol^{-1}). This points at an increased donor capability of the 1,2-azaboratabenzene subunit of **4** in comparison with the pyridine subunit of **3**. The enhanced electron sharing between Al and N in **4** was also mirrored by a Wiberg bond index (WBI) of 0.38. For pyridine **3**, this value was halved (WBI = 0.19), but a significant additional electron overlap was present between Al and the oxygen atom of the opposite monomer unit

(WBI = 0.18). This shows the strongly stabilizing effect of the dimerization, resulting from the pentacoordination of aluminum.

2.4. Optical Properties

Optical measurements were performed to quantify the impact of the BN vs. CN substitution. We representatively collected absorption and fluorescence emission spectra as well as quantum yields (Φ_{fl}) of dimethylaluminum complexes **3** and **4** (Figure 5). All BN complexes of boron and aluminum revealed similar fluorescence spectra, which was indicative of small contributions of the complexed ions on the excited states (see ESI, Figure S2).

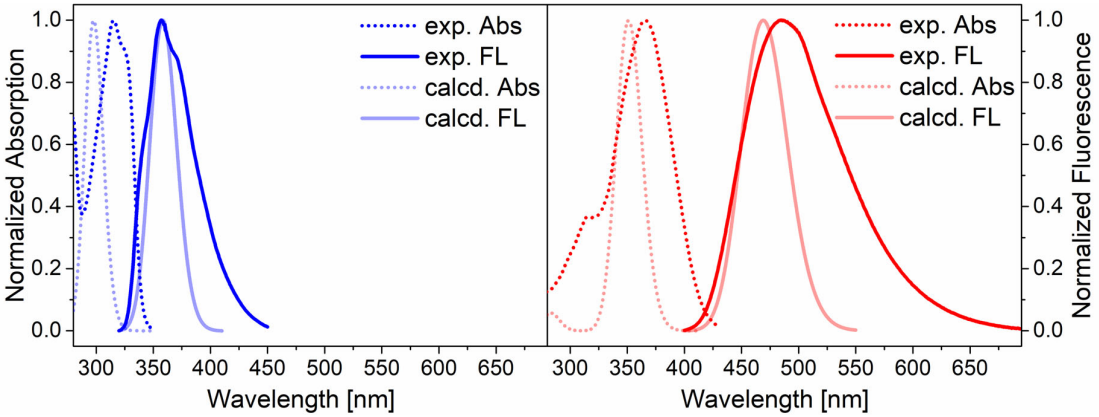

Figure 5. Experimental and theoretical absorption (dotted) and fluorescence (continuous) spectra of **4** (blue) and **3** (red) in benzene solutions. Scale of the x-axis defined by the UV cutoff at λ_{abs} = 280 nm.

The lowest-energy absorption band of BN complex **4** in benzene was located at λ_{abs} = 315 nm and for **3** at λ_{abs} = 365 nm. With respect to the fluorescence emission, **4** showed both a hypsochromic shift (λ_{fl} = 359 nm) compared to the CN congener **3** (λ_{fl} = 485 nm) and was less emissive (Φ_{fl} = 0.25 for **4**, Φ_{fl} = 0.50 for **3**). Moreover, the emission curve was narrowed significantly, and the Stokes shift (≈3900 cm^{-1}) was almost halved (**3**: ≈6800 cm^{-1}). By means of Time-Dependent DFT (TD-DFT) calculations using a Conductor-like Polarizable Continuum Model (CPCM) [42] with benzene as the solvent, we calculated the respective absorption and fluorescence spectra. For that purpose, monomeric CN complex **15** and anionic BN complex **14** were chosen because the optical properties of similar quinolinolates were practically independent of the coordination around Al [32]. Likewise, the lithium counterion should have a negligible effect at least in solution. All theoretically obtained spectra were in good agreement with the experimental ones ($\Delta\lambda$ < 17 nm, Figure 5), verifying that the theoretical model was suitable to map the electronic situations of both complexes also in the excited states.

The emission properties of quinolinolates are reportedly based on ligand-centered excited states, deriving from the lowest π–π* transitions within the ligands [43]. While the highest density of the highest occupied molecular orbitals (HOMOs) is predominantly at the phenol ring, the lowest unoccupied molecular orbitals (LUMOs) are rather centered at the pyridine ring [44].

By computing the Natural Transition Orbitals (NTOs) [45], a certain intraligand charge-transfer character between highest occupied (HONTO) and lowest unoccupied (LUNTO) NTOs in **[Me_2Al(Q')]** could be confirmed (Figure 6b, visualized using Visual Molecular Dynamics (VMD) [46]). On the other hand, the orbital distribution within **[Me_2Al(BQ)]**$^-$ was more uniform with similarly sized orbital lobes in both NTOs (Figure 6a). It has been described that a hypsochromic shift in emission can be achieved by installing electron donating substituents at the pyridine ring of hydroxyquinolines [47]. Therefore, the decreased emission wavelength of **4** could be attributable to the higher electron density within the azaborinine ring (see Section 2.3).

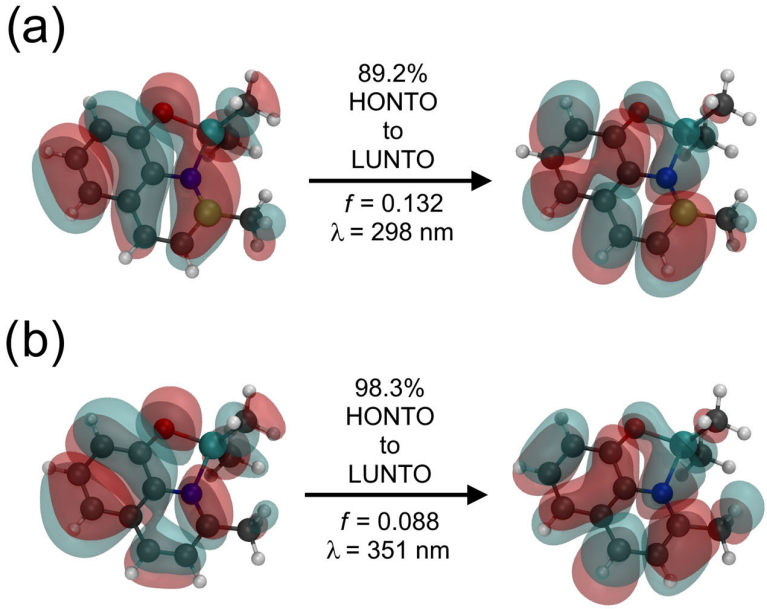

Figure 6. Representations of the main contributing NTOs to the S_1 states of **[Me_2Al(BQ)]**$^-$ (**a**) and **[Me_2Al(Q')]** (**b**) (iso values = 0.012). Also shown are the respective excitation energies and oscillator strengths *f*.

All depicted NTOs show little to no involvement of the aluminum atoms, confirming that π–π* transitions determine the optical properties of both complexes. Instead, we assume that the main impact of the aluminum atoms in both complexes is to rigidify the PAH cores and to suppress non-radiative deactivation pathways.

3. Materials and Methods

3.1. General Information

All syntheses and purification steps were performed using standard Schlenk techniques with argon as protective gas or with the aid of a nitrogen-filled glove box (Pure Lab^{HE} from Inert Innovative Technology Inc., Amesbury, MA, USA, <0.2 ppm O_2 and H_2O). Glassware and NMR tubes were heated to 110 °C under a vacuum below 0.1 mbar and flushed with argon at least three times prior to use. Syringes were flushed with argon at least three times prior to use. Complexations were performed in hermetically sealed NMR tubes, equipped with polytetrafluoroethylene (PTFE) valves (type PTFE500-5-7, Deutero GmbH, Kastellaun, Germany). All chemicals were purchased from commercial vendors. Reagents were degassed in a glove box evacuation chamber prior to the reaction (2-bromo-6-methoxyaniline, BLD Pharm, Shanghai, China, 97%; Cs_2CO_3, Carbolution, St. Ingbert, Germany, 99%; potassium methyltrifluoroborate, Apollo Sci., Stockport, UK; potassium vinyltrifluoroborate, BLD Pharm, 95%; 2-methyl-8-hydroxyquinoline, BLD Pharm, 99.8%) or stored in a glove box after degassing ($Pd(tBu_3P)_2$, Apollo Sci.; $SiCl_4$, Acros Organics, Geel, Belgium, 99.8%; BPh_3, Thermo Fisher Sci., Waltham, MA, USA, 96%; $NaBH_4$, abcr, Karlsruhe, Germany, 98%; triethylamine, Acros Organics, 99%; 1.0 M BEt_3 in THF, Thermo Fisher Sci.). Reagent solutions in sealed bottles were stored under argon at 5 °C (1.0 M BBr_3 in dichloromethane (DCM), Sigma Aldrich Chemie GmbH, Taufkirchen, Germany; 1.0 M $LiAlH_4$ in THF, Sigma Aldrich; 1.0 M LHMDS in THF, Sigma-Aldrich; 2.0 M $AlMe_3$ in hexanes, Sigma Aldrich; 1.0 M $AlPh_3$ in di-*n*-butyl ether, Sigma Aldrich). All solvents were dried prior to their use. Glassware and syringes containing highly pyrophoric R_3B and R_3Al species were rinsed with cyclohexane before deactivation with ethanol. Dry DCM (Merck, 99.5%), *n*-pentane (VWR, Radnor, PE, USA, 95%, distilled by rotary evaporation), THF (VWR, 99.7%) and toluene (Merck, 99.7%) were purified with an Inert PureSolv Micro Solvent Purification System (Inert Innovative Technology Inc., Amesbury, MA, USA). *n*-Hexane (Honeywell, Morristown, NJ, USA, 97%) was purified with an MB-SPS-800 sol-

vent purification system (M. Braun Inertgas-Systeme GmbH, Garching, Germany). CPME (Acros Organics, 99%), 1,4-dioxane (Honeywell, 99.5%), THF, THF-d_8 (Eurisotop, Saint-Aubin, France, 99.5% D) and *n*-hexane were stored over molecular sieves (3 Å) in a glove box. Using a Titroline 7500 KF Trace Karl-Fischer titrator (SI Analytics, Mainz, Germany), it was ensured that the water content of all solvents was <5 ppm. Chromatographic purifications were performed on sintered glass filters (*d*: 4 cm, *h*: 8 cm), using silica gel (Macherey-Nagel, Düren, Germany, particle size 0.015–0.040 mm). Thin-layer chromatography was performed on pre-coated silica gel 60 F_{254} plates. Spots were detected using a fluorescent lamp (λ = 254 or 365 nm). ^{1}H (601 MHz), ^{13}C{^{1}H} (151 MHz) and ^{11}B{^{1}H} (193 MHz) NMR spectra were recorded at 297 K on a Bruker AVANCE NEO 600 spectrometer (Bruker BioSpin, Rheinstetten, Germany). Chemical shifts (δ) are reported as parts per million (ppm) and are referenced against tetramethylsilane, the residual solvent signals (^{1}H, $CDCl_3$ at 7.26 ppm, THF-d_8 at 3.58 ppm) or the solvent itself (^{13}C{^{1}H}, $CDCl_3$ at 77.16 ppm, THF-d_8 at 67.57 ppm). Two-dimensional NMR experiments such as ^{1}H–^{1}H COSY, ^{1}H/^{13}C HSQC and ^{1}H/^{13}C HMBC were used to assign the signals. Hydrogen and carbon atoms of the aromatic backbones are labelled with letters to simplify their assignment. High resolution ESI mass spectra were recorded on a Bruker Impact II (Bruker Daltonics, Bremen, Germany). High resolution electron impact (EI) mass spectra were recorded on a double focusing mass spectrometer ThermoQuest Finnigan MAT95 XL (Thermo Fisher Sci.) at an ionization energy of 70 eV and a resolution R ≈ 10 000). IR spectra were recorded on a Nicolet iS20 FT-IR spectrometer with an attenuated total reflectance (ATR) unit (Thermo Fisher Sci.). All optical measurements were carried out using quartz cuvettes (optical path length: 1 cm). Absorption spectra were recorded on a Shimadzu UV-2700 spectrophotometer (Shimadzu Corp., Kyōto, Japan) with double monochromator. Fluorescence spectra were recorded on a Jasco FP-8300 spectrofluorometer (Jasco Corp., Tokyo, Japan). Fluorescence quantum yields (Φ) are double-corrected and were determined on the same instrument, using a Jasco ILF-835 integrating sphere. Melting points were measured on a Büchi M-560 Melting Point (Büchi, Flawil, Switzerland) device. X-ray diffraction measurements were performed at 100 or 120 K on a Bruker APEX-II CCD diffractometer (Bruker, Karlsruhe, Germany) with Mo-Kα (λ = 0.7107 Å) radiation. Air- and moisture sensitive single crystals suitable for X-ray diffraction analysis were grown in a glove box by slow diffusion of *n*-hexane. They were covered with cryoprotecting oil (Paratone) and then mounted on the diffractometer. Using OLEX2 [48], the structures were solved with the SHELXT [49] structure solution program using Intrinsic Phasing. Refinements were performed with the SHELXL [50] refinement package using Least Squares minimization. All non-hydrogen atoms were refined using anisotropic displacement parameters. Hydrogen atoms were included in geometrically calculated positions using a riding model. Crystal data are provided free of charge by the joint Cambridge Crystallographic Data Centre and Fachinformationszentrum Karlsruhe Access Structures service (www.ccdc.cam.ac.uk/structures). Figures were created using OLEX2.

*3.2. Synthesis of 2-Methoxy-6-vinylaniline (**6**)*

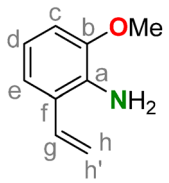

In a glove box, 2-bromo-6-methoxyaniline (**5**, 2.02 g, 10.0 mmol, 1.00 equiv.), potassium vinyltrifluoroborate (2.68 g, 20.0 mmol, 2.00 equiv., cesium carbonate (9.77 g, 30.0 mmol, 3.00 equiv.), Pd(tBu$_3$P)$_2$ (256 mg, 500 µmol, 5 mol%) and 1,4-dioxane (90 mL) were added to a pressure vessel. Outside the box, degassed water (10 mL) was added. The vessel was sealed with a PTFE cap and heated at 90 °C for 16 h in an oil bath. The mixture was filtered and washed with water (3 × 50 mL). The organic layer was dried over sodium sulfate. The solvent was removed under reduced pressure and the crude product was filtered over silica

(eluents: 10% *v*/*v* diethyl ether in cyclohexane, R_f = 0.28) to yield a yellow oil (1.26 g, 85%). **^{1}H NMR** (601 MHz, $CDCl_3$): δ = 6.96 (dd, ^3J = 6.5 Hz, ^4J = 2.6 Hz, 1H, e), 6.80 (dd, ^3J = 17.4, 11.1 Hz, 1H, g), 6.76–6.71 (m, 2H, c+d), 5.65 (dd, ^3J = 17.4 Hz, ^4J = 1.5 Hz, 1H, h), 5.32 (dd, ^3J = 11.1 Hz, ^4J = 1.5 Hz, 1H, h'), 3.96 (br s, 2H, NH_2), 3.86 (s, 3H, O-CH_3) ppm. **^{13}C{^{1}H} NMR** (151 MHz, $CDCl_3$): δ = 147.6 (b), 133.9 (a), 132.6 (g), 124.1 (f), 119.3 (e), 117.9 (d), 115.6 (h), 109.5 (c), 55.8 (O-CH_3) ppm. **IR**: $\tilde{\nu}$ [cm^{-1}] = 3463 (w), 3375 (w), 3082 (w), 3001 (w), 2936 (w), 2902 (w), 2835 (w), 1627 (m), 1613 (m), 1573 (m), 1471 (s), 1439 (m), 1276 (m), 1258 (s), 1234 (s), 1172 (m), 1050 (s), 991 (m), 906 (m), 785 (s), 731 (s), 698 (s). **HR-MS** (EI): *m*/*z* calc. for $C_9H_{11}NO$ 149.08352 $[M]^+$, found 149.08344 $[M]^+$ (100). **R_f** (silica, 10% *v*/*v* diethyl ether in cyclohexane) = 0.28.

*3.3. Synthesis of 8-Methoxy-2-methyl-1,2-dihydro-1-aza-2-boranaphthalene (**7**)*

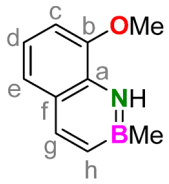

In a glove box, 2-methoxy-6-vinylaniline (**6**, 1.30 g, 8.71 mmol, 1.00 equiv.), potassium methyltrifluoroborate (1.17 g, 9.58 mmol, 1.10 equiv.), silicon tetrachloride (1.63 g, 9.58 mmol, 1.10 equiv.), triethylamine (1.32 g, 13.1 mmol, 1.50 equiv.), CPME (12 mL) and toluene (10 mL) were added to a sealable vessel. The resulting mixture was heated to 50 °C for 17 h. The solvents were removed in vacuo. The crude product was purified by filtration over silica (eluent: DCM) to yield a yellow oil (890 mg, 59%). **^{1}H NMR** (601 MHz, $CDCl_3$): δ = 8.37 (app br s, 1H, N*H*) (Apparent Broad Singlet. ^4J Coupling to h is Not Visible), 7.91 (d, ^3J = 11.4 Hz, 1H, g), 7.21 (app d, ^3J = 7.9 Hz, 1H, e) (Apparent Doublet. ^4J Coupling Only Visible in ^{1}H–^{1}H COSY NMR), 7.04 (dd, ^3J = 7.9, 7.9 Hz, 1H, d), 6.91 (dd, ^3J = 7.9 Hz, ^4J = 1.2 Hz, 1H, c), 6.83 (dd, ^3J = 11.4 Hz, ^4J = 2.0 Hz, 1H, h), 4.00 (s, 3H, O-CH_3), 0.77 (s, 3H, B-CH_3) ppm. **^{13}C{^{1}H} NMR** (151 MHz, $CDCl_3$): δ = 147.6 (b), 143.6 (g), 131.5 (h), 131.1 (a), 125.4 (f), 121.4 (e), 119.6 (d), 107.7 (c), 55.9 (O-CH_3), 2.5 (B-CH_3) ppm. **^{11}B{^{1}H} NMR** (193 MHz, $CDCl_3$): δ = 37.3 ppm. **IR**: $\tilde{\nu}$ [cm^{-1}] = 3402 (w), 3010 (w), 2937 (w), 2841 (w), 1619 (m), 1600 (w), 1563 (s), 1457 (m), 1441 (m), 1431 (m), 1394 (m), 1364 (m), 1256 (s), 1223 (m), 1131 (m), 1075 (s), 885 (m), 816 (m), 762 (m), 739 (s), 698 (m). **HR-MS** (EI): *m*/*z* calc. for $C_{10}H_{12}{}^{11}BNO$ 173.10083 $[M]^+$, found 173.10068 $[M]^+$ (100). **R_f** (silica, 2% *v*/*v* diethyl ether in cyclohexane) = 0.46.

*3.4. Synthesis of 8-Hydroxy-2-methyl-1,2-dihydro-1-aza-2-boranaphthalene (**1**)*

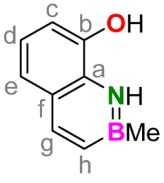

Under argon, 8-methoxy-2-methyl-1,2-dihydro-1-aza-2-boranaphthalene (**7**, 567 mg, 3.28 mmol) was dissolved in DCM (30 mL) and cooled to 0 °C. A boron tribromide solution (13.1 mL, 13.1 mmol, 1.00 M) was added dropwise over the course of 10 min. The mixture was stirred at 0 °C for 90 min and subsequently poured into ice water (200 mL). DCM (100 mL) was added, and the mixture was stirred for 30 min at 25 °C. The phases were separated. The aqueous layer was extracted with DCM (3 × 50 mL). The combined organic phases were dried over sodium sulfate. After filtration and evaporation of the volatiles in vacuo, the crude product was purified by filtration over silica (eluents: 20% *v*/*v* diethyl ether in cyclohexane). A yellow oil (299 mg, 57%) was obtained, that slowly solidified at 25 °C. **^{1}H NMR** (601 MHz, THF-d_8): δ = 8.88 (s, 1H, O*H*), 8.65 (br s, 1H, N*H*), 7.84 (d, ^3J = 11.4 Hz, 1H, g), 7.04 (app d, ^3J = 7.9 Hz, 1H, e) (Apparent Doublet. ^4J Coupling Only Visible in ^{1}H–^{1}H COSY NMR), 6.85 (dd, ^3J = 7.9, 7.9 Hz, 1H, d), 6.78 (dd, ^3J = 7.9 Hz,

^4J = 1.3 Hz, 1H, c), 6.71 (dd, ^3J = 11.4 Hz, ^4J = 2.0 Hz, 1H, h), 0.72 (s, 3H, B-CH_3) ppm. **^{13}C{^{1}H} NMR** (151 MHz, THF-d_8): δ = 146.2 (b), 144.7 (g), 131.8 (a+h), 127.0 (f), 121.0 (e), 120.5 (d), 112.4 (c), 1.5 (B-CH_3) ppm. **^{11}B{^{1}H} NMR** (193 MHz, THF-d_8): δ = 37.3 ppm. **IR**: $\tilde{\nu}$ [cm^{-1}] = 3398 (m), 3314 (m, br), 3007 (w), 2940 (w), 2899 (w), 1626 (m), 1600 (w), 1564 (s), 1459 (m), 1431 (s), 1393 (m), 1309 (m), 1253 (s), 1204 (m), 1156 (m), 1122 (s), 1008 (s), 946 (m), 880 (s), 870 (m), 835 (m), 815 (m), 735 (s), 711 (s), 694 (s). **m.p.**: 47 °C. **HR-MS** (ESI negative, methanol): *m/z* calc. for $C_9H_9{}^{11}BNO$ 158.07827 [M-H]$^-$, found 158.07804 [M-H]$^-$ (100). **R_f** (silica, 20% *v*/*v* diethyl ether in cyclohexane) = 0.43.

3.5. General Procedure for the Complexation of Group 13 Elements

Under Schlenk conditions, **1** (15.9 mg, 100 µmol, 1.00 equiv.) was dissolved in a mixture of 1,4-dioxane (400 µL) and THF-d_8 (100 µL) in a sealable NMR tube. If denoted, a solution of LHMDS (250 µL, 250 µmol, 2.50 equiv., 1.0 M) was added with a syringe and the quantitative conversion into **8** was confirmed by ^{1}H NMR spectroscopy. Afterwards, the respective group 13 reagent was added. The mixture was subjected to the specified temperature/time protocol. Upon full conversion, the complexes were isolated in a glove box as described for the individual compounds.

*3.6. 1:1. Complex of **H_2(BQ)** with Triethylborane (**Li[Et_2B(BQ)]**)*

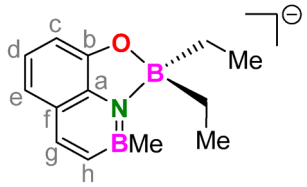

Initial deprotonation. Reagent: BEt_3 (250 µL, 250 µmol, 2.50 equiv., 1.00 M), heated at 130 °C for 17 h. Workup: In a glove box, *n*-hexane was allowed to diffuse into the crude reaction mixture over the course of 14 d. The upper solvent layer was transferred to a vial and over the course of 14 d, colorless crystals suitable for X-ray diffraction analysis formed at the edge of the vial. The residue was extracted with a mixture of 10% THF in *n*-pentane (3 × 2 mL). The product was obtained as a brown oil (74.0 mg) and was contaminated with $LiBEt_4$. **^{1}H NMR** (601 MHz, THF-d_8): δ = 7.55 (d, ^3J = 10.9 Hz, 1H, g), 6.61 (dd, ^3J = 8.0 Hz, ^4J = 0.9 Hz, 1H, e), 6.52–6.46 (m, 2H, d+h), 6.22 (app d, ^3J = 7.3 Hz, 1H, c) (Apparent Doublet. ^4J Coupling Only Visible in ^{1}H–^{1}H COSY NMR), 0.63–0.55 (m, 7H, B-CH_3 + B-CH_2-CH_3), 0.51 (t, ^3J = 7.4 Hz, 6H, B-CH_2-CH_3) ppm. **^{13}C{^{1}H} NMR** (151 MHz, THF-d_8): δ = 157.4 (b), 142.9 (a), 139.7 (g), 132.5 (h), 124.3 (f), 118.3 (e), 115.9 (d), 103.4 (c), 17.1 (B-CH_2-CH_3), 9.8 (B-CH_2-CH_3), 3.0 (B-CH_3) ppm. **^{11}B{^{1}H} NMR** (193 MHz, THF-d_8): δ = 35.9 (azaborinine), 13.3 (complexed) ppm. **HR-MS** (ESI negative, THF): *m/z* calc. for $C_{13}H_{18}{}^{11}B_2NO$ 226.15800 **[Et_2B(BQ)]**$^-$, found 226.15863 **[Et_2B(BQ)]**$^-$. Crystal data for **([Li(THF)$_2$(diox)$_{0.5}$][Et_2B(BQ)])$_2$** ($C_{46}H_{76}B_4Li_2N_2O_8$, *M* = 842.20 g/mol): monoclinic, space group $P2_1/c$ (no. 14), *a* = 9.796(3) Å, *b* = 14.727(4) Å, *c* = 17.458(4) Å, β = 103.832(12)°, *V* = 2445.6(12) Å^3, *Z* = 2, *T* = 100.00 K, µ(Mo-Kα) = 0.074 mm^{-1}, *Dcalc* = 1.144 g/cm^3, 10,969 reflections measured (4.806° ≤ 2Θ ≤ 51.36°), 4594 unique (R_{int} = 0.0880, R_{sigma} = 0.1200) which were used in all calculations. The final R_1 was 0.0770 (I > 2σ(I)) and wR_2 was 0.2302 (all data). CCDC deposition number: 2259514.

3.7. 1:1. Complex of H_2(BQ) with Triphenylborane (Li[Ph_2B(BQ)])

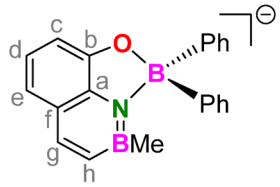

Initial deprotonation. Reagent: BPh_3 (60.5 mg, 250 µmol, 2.50 equiv.), heated at 130 °C for 17 h. Workup: In a glove box, the volatiles were removed in vacuo. The crude was washed with a mixture of 10% THF in *n*-pentane (5 mL). Subsequently, it was extracted with a mixture of 30% THF in *n*-pentane (5 × 2 mL). Evaporation of the solvents yielded the product as a colorless solid (16.5 mg, 30%). Colorless crystals suitable for X-ray diffraction analysis were obtained by diffusion of *n*-hexane into a solution of the complex in THF over the course of 7 d. **^{1}H NMR** (601 MHz, THF-d_8): δ = 7.68 (d, ^3J = 11.0 Hz, 1H, g), 7.39 (d, ^3J = 7.3 Hz, 4H, *o*-C*H*), 7.03 (dd, ^3J = 7.3, 7.3 Hz, 4H, *m*-C*H*), 6.96 (t, ^3J = 7.3 Hz, 2H, *p*-C*H*), 6.78 (d, ^3J = 8.1 Hz, 1H, e), 6.60 (dd, ^3J = 8.1, 7.3 Hz, 1H, d), 6.56 (d, ^3J = 11.0 Hz, 1H, h), 6.33 (d, ^3J = 7.3 Hz, 1H, c), 0.23 (s, 3H, B-CH_3) ppm. **^{13}C{^{1}H} NMR** (151 MHz, THF-d_8): δ = 155.8 (b), 153.0 (C_q), 141.9 (a), 140.3 (g), 134.9 (*o*-CH), 133.6 (h), 127.1 (*m*-CH), 125.7 (*p*-CH), 124.6 (f), 118.9 (e), 117.0 (d), 104.6 (c), 4.0 (B-CH_3) ppm. **^{11}B{^{1}H} NMR** (193 MHz, THF-d_8): δ = 37.3 (azaborinine), 10.5 (complexed) ppm. **HR-MS** (ESI negative, THF): *m/z* calc. for $C_{21}H_{18}{}^{11}B_2NO$ 322.15800 **[Ph$_2$B(BQ)]$^-$**, found 322.15896 **[Ph$_2$B(BQ)]$^-$**. Crystal data for **[Li(THF)$_3$][Ph$_2$B(BQ)]** ($C_{33}H_{42}B_2LiNO_4$, *M* = 545.23 g/mol): monoclinic, space group $P2_1/c$ (no. 14), *a* = 17.6018(8) Å, *b* = 20.7780(12) Å, *c* = 16.8289(9) Å, *β* = 90.789(2)°, *V* = 6154.3(6) Å^3, *Z* = 8, *T* = 100.00 K, µ(Mo-K*α*) = 0.074 mm^{-1}, *Dcalc* = 1.177 g/cm^3, 338,940 reflections measured (3.86° ≤ 2Θ ≤ 56.646°), 15,347 unique (R_{int} = 0.0825, R_{sigma} = 0.0261) which were used in all calculations. The final R_1 was 0.0646 (I > 2σ(I)) and wR_2 was 0.1619 (all data). CCDC deposition number: 2259522.

*3.8. 2:1. Complex of **H$_2$(BQ)** with Sodium Borohydride (**Na[B(BQ)$_2$]**)*

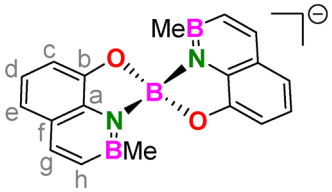

No initial deprotonation. Reagent: $NaBH_4$ (9.5 mg, 250 µmol, 2.50 equiv.), heated at 130 °C for 6 d. Workup: In a glove box, the precipitated excess of $NaBH_4$ was removed using a syringe filter (pore size: 0.40 µm). The solvents were removed in vacuo, giving a yellow solid. The crude product was extracted with a mixture of 3% THF in *n*-pentane (3 × 2 mL). Evaporation of the solvents yielded the product as a colorless solid (20.0 mg, 41%). Colorless needles suitable for X-ray diffraction analysis were obtained by diffusion of *n*-hexane into a solution of the complex in THF over the course of 7 d. **^{1}H NMR** (601 MHz, THF-d_8): δ = 7.72 (d, ^3J = 11.1 Hz, 2H, g), 6.89 (dd, ^3J = 8.2 Hz, ^4J = 1.0 Hz, 2H, e), 6.75 (dd, ^3J = 8.2, 7.3 Hz, 2H, d), 6.57 (app d, ^3J = 7.3 Hz, 2H, c) (Apparent Doublet. ^4J Coupling Only Visible in ^{1}H–^{1}H COSY NMR), 6.54 (d, ^3J = 11.1 Hz, 2H, h), −0.05 (s, 6H, B-CH_3) ppm. **^{13}C{^{1}H} NMR** (151 MHz, THF-d_8): δ = 153.7 (b), 141.5 (g), 140.3 (a), 133.4 (h), 123.3 (f), 119.5 (e), 117.5 (d), 105.6 (c), 1.5 (B-CH_3) ppm. **^{11}B{^{1}H} NMR** (193 MHz, THF-d_8): δ = 38.4 (azaborinine), 15.2 (complexed) ppm. **HR-MS** (ESI negative, THF): *m/z* calc. for $C_{18}H_{16}{}^{11}B_3N_2O_2$ 325.14964 **[B(BQ)$_2$]$^-$**, found 325.15115 **[B(BQ)$_2$]$^-$**. Crystal data for **([Na(THF)$_2$][B(BQ)$_2$])$_2$** ($C_{26}H_{32}B_3N_2NaO_4$, *M* = 491.95 g/mol): triclinic, space group P-1 (no. 2), *a* = 11.1607(19) Å, *b* = 11.892(2) Å, *c* = 12.316(2) Å, *α* = 117.706(6)°, *β* = 92.755(6)°, *γ* = 110.342(6)°, *V* = 1313.0(4) Å^3, *Z* = 2, *T* = 119.99 K, µ(Mo-K*α*) = 0.095 mm^{-1}, *Dcalc* = 1.244 g/cm^3, 36,401 reflections measured (4.822° ≤ 2Θ ≤ 56.712°), 6557 unique (R_{int} = 0.0508, R_{sigma} = 0.0353) which were used in all calculations. The final R_1 was 0.0503 (I > 2σ(I)) and wR_2 was 0.1288 (all data). CCDC deposition number: 2259516.

3.9. 1:1. Complex of $H_2(BQ)$ *with Trimethylaluminum (*$Li[Me_2Al(BQ)]$*)*

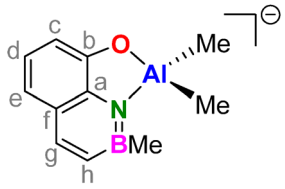

Initial deprotonation. Reagent: $AlMe_3$ (125 µL, 250 µmol, 2.50 equiv., 2.0 M), no heating required. Workup: In a glove box, *n*-hexane was allowed to diffuse into the crude reaction mixture. Over the course of 14 d, large colorless crystals formed, which were collected and washed with *n*-pentane (2 × 2 mL). These crystals (35.4 mg, 81%) were also suitable for X-ray diffraction analysis. **^{1}H NMR** (601 MHz, THF-d_8): δ = 7.64 (d, ^3J = 11.2 Hz, 1H, g), 6.73 (dd, ^3J = 8.0 Hz, ^4J = 1.2 Hz, 1H, e), 6.58–6.50 (m, 2H, d+h), 6.43 (dd, ^3J = 7.5 Hz, ^4J = 1.2 Hz, 1H, c), 0.64 (s, 3H, B-CH_3), −0.85 (s, 6H, Al-CH_3) ppm. **^{13}C{^{1}H} NMR** (151 MHz, THF-d_8): δ = 155.5 (b), 142.7 (a), 142.6 (g), 131.9 (h), 126.8 (f), 118.4 (e), 117.8 (d), 109.1 (c), 4.6 (B-CH_3), −7.9 (Al-CH_3) ppm. **^{11}B{^{1}H} NMR** (193 MHz, THF-d_8): δ = 37.3 ppm. **HR-MS** (ESI negative, THF): *m/z* calc. for $C_{11}H_{14}Al^{11}BNO$ 214.09893 **[Me$_2$Al(BQ)]**$^-$, found 214.09856 **[Me$_2$Al(BQ)]**$^-$. Crystal data for **[Li(THF)$_3$][Me$_2$Al(BQ)]** ($C_{23}H_{38}AlBLiNO_4$, *M* = 437.27 g/mol): monoclinic, space group Cc (no. 9), *a* = 17.801(3) Å, *b* = 8.5125(13) Å, *c* = 18.438(4) Å, *β* = 114.105(13)°, *V* = 2550.4(8) Å^3, *Z* = 4, *T* = 100.00 K, µ(Mo-Kα) = 0.106 mm^{-1}, *Dcalc* = 1.139 g/cm^3, 35,381 reflections measured (4.84° ≤ 2Θ ≤ 61.138°), 7388 unique (R_{int} = 0.0504, R_{sigma} = 0.0436) which were used in all calculations. The final R_1 was 0.0370 (I > 2σ(I)) and wR_2 was 0.0811 (all data). CCDC deposition number: 2259515.

3.10. 1:1. Complex of $H_2(BQ)$ *with Triphenylaluminum (*$Li[Ph_2Al(BQ)]$*)*

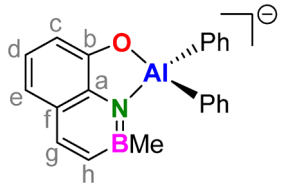

Initial deprotonation. Reagent: $AlPh_3$ (100 µL, 100 µmol, 1.00 equiv., 1.0 M), no heating required. Workup: In a glove box, the volatiles were removed in vacuo. The crude was washed with a mixture of 10% THF in n-pentane (2 × 2 mL). Drying it in vacuo resulted in a beige solid (29.8 mg, 53%). Colorless needles suitable for X-ray diffraction analysis were obtained by diffusion of *n*-hexane into a solution of the complex in THF over the course of 7 d. **^{1}H NMR** (601 MHz, THF-d_8): δ = 7.73 (d, ^3J = 11.2 Hz, 1H, g), 7.69–7.64 (m, 4H, *o*-C*H*), 7.11–7.04 (m, 6H, *m*-C*H*, *p*-C*H*), 6.85 (dd, ^3J = 7.9 Hz, ^4J = 1.3 Hz, 1H, e), 6.67 (dd, ^3J = 7.9, 7.5 Hz, 1H, d), 6.62 (dd, ^3J = 7.5 Hz, ^4J = 1.3 Hz, 1H, c), 6.57 (d, ^3J = 11.2 Hz, 1H, h), 0.50 (s, 3H, B-CH_3) ppm. **^{13}C{^{1}H} NMR** (151 MHz, THF-d_8): δ = 155.4 (b), 151.2 (C_q), 142.9 (g), 142.8 (a), 139.1 (*o*-CH), 132.0 (h), 127.5 (*p*-CH), 127.2 (*m*-CH), 126.9 (f), 118.7 (e), 118.3 (d), 109.7 (c), 5.3 (B-CH_3) ppm. **^{11}B{^{1}H} NMR** (193 MHz, THF-d_8): δ = 39.6 ppm. **HR-MS** (ESI negative, THF): *m/z* calc. for $C_{21}H_{18}Al^{11}BNO$ 338.13023 **[Ph$_2$Al(BQ)]**$^-$, found 338.13016 **[Ph$_2$Al(BQ)]**$^-$. Crystal data for **[Li(THF)$_3$][Ph$_2$Al(BQ)]** $C_{33}H_{42}AlBLiNO_4$, *M* = 561.40 g/mol): orthorhombic, space group $Pca2_1$ (no. 29), *a* = 17.6861(10) Å, *b* = 9.5637(6) Å, *c* = 18.7543(19) Å, *V* = 3172.2(4) Å^3, *Z* = 4, *T* = 100.00 K, µ(Mo-Kα) = 0.100 mm^{-1}, *Dcalc* = 1.176 g/cm^3, 69,045 reflections measured (4.606° ≤ 2Θ ≤ 61.08°), 9687 unique (R_{int} = 0.0627, R_{sigma} = 0.0417) which were used in all calculations. The final R_1 was 0.0599 (I > 2σ(I)) and wR_2 was 0.1761 (all data). CCDC deposition number: 2259521.

3.11. 2:1. Complex of $H_2(BQ)$ *with Lithium Aluminum Hydride (*$Li[Al(BQ)_2]$*)*

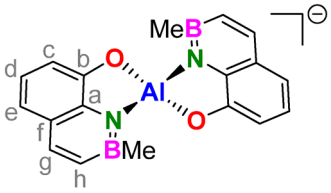

No initial deprotonation. Reagent: $LiAlH_4$ (50.0 µL, 50.0 µmol, 0.50 equiv., 1.0 M), heated at 130 °C for 17 h. Workup: In a glove box, the solvent was removed in vacuo and the product was obtained as a colorless solid (19.6 mg, 69%). Single crystals suitable for X-ray diffraction analysis were obtained via diffusion of *n*-hexane into a solution of the complex in THF over the course of 7 d. **^{1}H NMR** (601 MHz, THF-d_8): δ = 7.77 (d, ^3J = 11.3 Hz, 2H, g), 6.90 (dd, ^3J = 7.7 Hz, ^4J = 1.3 Hz, 2H, e), 6.76 (dd, ^3J = 7.7 Hz, 2H, d), 6.70 (dd, ^3J = 7.7 Hz, ^4J = 1.3 Hz, 2H, c), 6.58 (d, ^3J = 11.3 Hz, 2H, h), 0.33 (s, 6H, B-CH_3) ppm. **^{13}C{^{1}H} NMR** (151 MHz, THF-d_8): δ = 153.5 (b), 143.9 (g), 141.4 (a), 131.8 (h), 126.5 (f), 119.5 (d), 118.9 (e), 110.8 (c), 4.6 (B-CH_3) ppm. **^{11}B{^{1}H} NMR** (193 MHz, THF-d_8): δ = 38.9 ppm. Crystal data for **$[Li(THF)_3][Al(BQ)_2]$** ($C_{30}H_{40}AlB_2LiN_2O_5$, *M* = 564.18 g/mol): triclinic, space group P-1 (no. 2), *a* = 10.070(3) Å, *b* = 10.701(3) Å, *c* = 15.809(5) Å, α = 85.336(11)°, β = 81.473(12)°, γ = 64.072(9)°, *V* = 1515.0(8) Å^3, *Z* = 2, *T* = 100.00 K, µ(Mo-Kα) = 0.108 mm^{-1}, *Dcalc* = 1.237 g/cm^3, 29,381 reflections measured (4.232° ≤ 2Θ ≤ 56.706°), 7543 unique (R_{int} = 0.0730, R_{sigma} = 0.0675) which were used in all calculations. The final R_1 was 0.0559 (I > 2σ(I)) and wR_2 was 0.1236 (all data). CCDC deposition number: 2259518.

3.12. 1:1. Complex of HQ′ with Trimethylaluminum ($[Me_2Al(Q')]_2$*)*

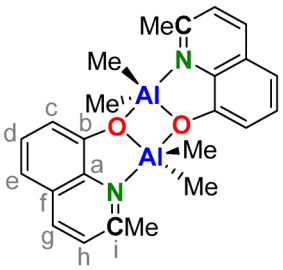

In a Schlenk tube at 25 °C, $AlMe_3$ (600 µL, 1.20 mmol, 1.20 equiv., 2.0 M) was dissolved in toluene (5 mL). A solution of 2-methyl-8-hydroxyquinoline (**HQ′**, 159 mg, 1.00 mmol, 1.00 equiv.) in toluene (5 mL) was added dropwise over the course of 5 min. The clear solution was stirred at the same temperature for 17 h, after which a colorless precipitation had formed. The latter was filtered over a frit in a glove box and washed with toluene (2 × 5 mL). After drying on a Schlenk line (80 °C, 0.10 mbar, 2 h), the product was obtained as a colorless solid (162 mg, 75%). **^{1}H NMR** (601 MHz, $CDCl_3$): δ = 8.20 (d, ^3J = 8.4 Hz, 2H, g), 7.50 (dd, ^3J = 8.2, 7.5 Hz, 2H, d), 7.37 (d, ^3J = 8.4 Hz, 2H, h), 7.34 (d, ^3J = 7.5 Hz, 2H, c), 7.30 (d, ^3J = 8.2 Hz, 2H, e), 2.91 (s, 6H, C-CH_3), –0.57 (s, 12H, Al-CH_3) ppm. **^{13}C{^{1}H} NMR** (151 MHz, $CDCl_3$): δ = 156.0 (i), 138.5 (g), 128.6 (d), 127.2 (f), 124.2 (h), 116.2 (e), 113.5 (c), 23.0 (C-CH_3), –7.6 (Al-CH_3) ppm. Carbon atoms a and b not detected. **IR**: $\tilde{\nu}$ [cm^{-1}] = 2948 (w), 2926 (w), 2885 (w), 2824 (w), 1615 (w), 1604 (w), 1578 (m), 1507 (m), 1472 (m), 1431 (m), 1396 (m), 1330 (m), 1265 (m), 1243 (m), 1188 (m), 1108 (m), 828 (m), 795 (w), 752 (s), 671 (s), 662 (s). **m.p.**: Decomposition onset at 210 °C, residue melts at 255 °C. **HR-MS** (EI): *m/z* calc. for $C_{12}H_{14}AlNO$ 215.08853 [M]$^+$, found 215.08895 [M]$^+$ (4), 200.1 (100). Crystal data for **$[Me_2Al(Q')]$** ($C_{12}H_{14}AlNO$, *M* = 215.22 g/mol): triclinic, space group P-1 (no. 2), *a* = 9.537(3) Å, *b* = 9.792(2) Å, *c* = 12.638(3) Å, α = 88.302(9)°, β = 73.190(10)°, γ = 81.824(9)°, *V* = 1118.1(5) Å^3, *Z* = 4, *T* = 100.00 K, µ(Mo-Kα) = 0.153 mm^{-1}, *Dcalc* = 1.279 g/cm^3, 71,748 reflections measured (5.718° ≤ 2Θ ≤ 61.088°), 6824 unique (R_{int} = 0.0508, R_{sigma} = 0.0272) which were used in all calculations. The final R_1 was 0.0353 (I > 2σ(I)) and wR_2 was 0.1076 (all data). CCDC deposition number: 2259520.

4. Conclusions

In summary, we have synthesized six coordination complexes of boron and aluminum with an *N,O*-donating 1,2-azaborinine ligand. By means of X-ray diffraction analysis, the high planarity of the PAH scaffolds as well as the tetrahedral geometries around the central ions were confirmed. Moreover, both the presence of boron instead of aluminum and a 2:1 instead of a 1:1 stoichiometry caused smaller N,O–E bond lengths. A multi-dimensional comparison of azaborinine complex **Li[Me$_2$Al(BQ)]** (**4**) and pyridine analog **[Me$_2$Al(Q')]$_2$** (**3**) allowed us to draw several conclusions on the influence of a B vs. C substitution. In particular, the presence of electropositive boron in **4** rendered the adjacent nitrogen donor atom more negative in charge (Δ of Natural Atomic Charges = 0.51). As the result, the N–Al donor–acceptor orbital interactions were strengthened, which complies with the shortened bond (Δd = 0.22 Å). The high charges at the phenolic oxygen atoms of both complexes were stabilized in different manners. While BN complex **4** has the counterion in close proximity, neutral CN complex **3** dimerizes to form a four-membered ring consisting of Al and O. From NTO analysis, the partial charge-transfer character of the S_1 state of quinolinolate **3** was demonstrated. BN analog **4** showed a more balanced distribution of the NTOs, which correlates with the experimentally obtained blueshifted absorption and emission bands ($\Delta\lambda_{fl}$ = 126 nm). Overall, our study emphasizes that the doping of quinolinolate ligands with a single boron atom may alter the electronic structure considerably, which has direct implications on the *N*-donor capability and the optical properties.

Supplementary Materials: The following supporting information can be downloaded at: https://www.mdpi.com/article/10.3390/inorganics11070295/s1, study of the hydrolytic stability, crystallographic details, copies of all NMR spectra, fluorescence spectra, computational details. Figure S1: Molecular structure of the monomeric unit and the dimer of **[Al(H(BQ))$_3$(THF)]$_2$**; Figure S2: Fluorescence emission spectra of **H$_2$(BQ)** and its complexes with boron and aluminum in THF solutions. Table S1: Crystal Data and Structure Refinements. Table S2: Coordinates of the geometry-optimized structures. Reference [51] is cited in the supplementary materials.

Author Contributions: Conceptualization, Y.A. and A.S.; methodology, Y.A. and J.W.; validation, Y.A. and J.W.; formal analysis, Y.A., P.P. and J.W.; investigation, Y.A., P.P. and J.W.; resources, T.N. and A.S.; data curation, Y.A. and P.P.; writing—original draft preparation, Y.A.; writing—review and editing, Y.A., P.P., J.W., T.N. and A.S.; visualization, Y.A. and J.W.; supervision, T.N. and A.S.; project administration, A.S. All authors have read and agreed to the published version of the manuscript.

Funding: This research received no external funding.

Data Availability Statement: The data presented in this study are openly available in the Supplementary Information.

Conflicts of Interest: The authors declare no conflict of interest.

References

1. Campbell, P.G.; Marwitz, A.J.V.; Liu, S.-Y. Recent Advances in Azaborine Chemistry. *Angew. Chem. Int. Ed.* **2012**, *51*, 6074–6092. [CrossRef]
2. Bélanger-Chabot, G.; Braunschweig, H.; Roy, D.K. Recent Developments in Azaborinine Chemistry. *Eur. J. Inorg. Chem.* **2017**, *38–39*, 4353–4368. [CrossRef]
3. Campbell, P.G.; Abbey, E.R.; Neiner, D.; Grant, D.J.; Dixon, D.A.; Liu, S.-Y. Resonance Stabilization Energy of 1,2-Azaborines: A Quantitative Experimental Study by Reaction Calorimetry. *J. Am. Chem. Soc.* **2010**, *132*, 18048–18050. [CrossRef] [PubMed]
4. Abbey, E.R.; Zakharov, L.N.; Liu, S.-Y. Crystal Clear Structural Evidence for Electron Delocalization in 1,2-Dihydro-1,2-azaborines. *J. Am. Chem. Soc.* **2008**, *130*, 7250–7252. [CrossRef]
5. Appiarius, Y.; Staubitz, A. Azaborinine. *Chem. Unserer Zeit* **2023**, *57*, 180–190. [CrossRef]
6. McConnell, C.R.; Liu, S.-Y. Late-stage functionalization of BN-heterocycles. *Chem. Soc. Rev.* **2019**, *48*, 3436–3453. [CrossRef] [PubMed]
7. Appiarius, Y.; Stauch, T.; Lork, E.; Rusch, P.; Bigall, N.C.; Staubitz, A. From a 1,2-azaborinine to large *BN*-PAHs via electrophilic cyclization: Synthesis, characterization and promising optical properties. *Org. Chem. Front.* **2021**, *8*, 10–17. [CrossRef]
8. Appiarius, Y.; Gliese, P.J.; Segler, S.A.W.; Rusch, P.; Zhang, J.; Gates, P.J.; Pal, R.; Malaspina, L.A.; Sugimoto, K.; Neudecker, T.; et al. BN-Substitution in Dithienylpyrenes Prevents Excimer Formation in Solution and in the Solid State. *J. Phys. Chem. C* **2022**, *126*, 4563–4576. [CrossRef]

9. Dewar, M.J.S.; Dietz, R. New heteroaromatic compounds. Part III. 2,1-Borazaro-naphthalene (1,2-dihydro-1-aza-2-boranaphthalene). *J. Chem. Soc.* **1959**, *546*, 2728–2730. [CrossRef]
10. Paetzold, P.; Stanescu, C.; Stubenrauch, J.R.; Bienmüller, M.; Englert, U. 1-Azonia-2-boratanaphthalenes. *Z. Anorg. Allg. Chem.* **2004**, *630*, 2632–2640. [CrossRef]
11. Wisniewski, S.R.; Guenther, C.L.; Argintaru, O.A.; Molander, G.A. A Convergent, Modular Approach to Functionalized 2,1-Borazaronaphthalenes from 2-Aminostyrenes and Potassium Organotrifluoroborates. *J. Org. Chem.* **2014**, *79*, 365–378. [CrossRef]
12. Liu, Z.; Ishibashi, J.S.A.; Darrigan, C.; Dargelos, A.; Chrostowska, A.; Li, B.; Vasiliu, M.; Dixon, D.A.; Liu, S.-Y. The Least Stable Isomer of BN Naphthalene: Toward Predictive Trends for the Optoelectronic Properties of BN Acenes. *J. Am. Chem. Soc.* **2017**, *139*, 6082–6085. [CrossRef] [PubMed]
13. Pan, J.; Kampf, J.W.; Ashe, A.J. 1,2-Azaboratabenzene: A Heterocyclic π-Ligand with an Adjustable Basicity at Nitrogen. *Organometallics* **2004**, *23*, 5626–5629. [CrossRef]
14. Pan, J.; Kampf, J.W.; Ashe Iii, A.J. The Preparation and Crystal Structures of η^1-Derivatives of 2-Phenyl-1,2-azaboratabenzene. *Organometallics* **2008**, *27*, 1345–1347. [CrossRef]
15. Lindl, F.; Lamprecht, A.; Arrowsmith, M.; Khitro, E.; Rempel, A.; Dietz, M.; Wellnitz, T.; Bélanger-Chabot, G.; Stoy, A.; Paprocki, V.; et al. Aromatic 1,2-Azaborinin-1-yls as Electron-Withdrawing Anionic Nitrogen Ligands for Main Group Elements. *Chem. Eur. J.* **2023**, *29*, e202203345. [CrossRef]
16. Baschieri, A.; Aleotti, F.; Matteucci, E.; Sambri, L.; Mancinelli, M.; Mazzanti, A.; Leoni, E.; Armaroli, N.; Monti, F. A Pyridyl-1,2-azaborine Ligand for Phosphorescent Neutral Iridium(III) Complexes. *Inorg. Chem.* **2023**, *62*, 2456–2469. [CrossRef]
17. Baggett, A.W.; Vasiliu, M.; Li, B.; Dixon, D.A.; Liu, S.-Y. Late-Stage Functionalization of 1,2-Dihydro-1,2-azaborines via Regioselective Iridium-Catalyzed C–H Borylation: The Development of a New N,N-Bidentate Ligand Scaffold. *J. Am. Chem. Soc.* **2015**, *137*, 5536–5541. [CrossRef] [PubMed]
18. Linnell, R. Notes- Dissociation Constants of 2-Substituted Pyridines. *J. Org. Chem.* **1960**, *25*, 290. [CrossRef]
19. Davies, G.H.M.; Jouffroy, M.; Sherafat, F.; Saeednia, B.; Howshall, C.; Molander, G.A. Regioselective Diversification of 2,1-Borazaronaphthalenes: Unlocking Isosteric Space via C–H Activation. *J. Org. Chem.* **2017**, *82*, 8072–8084. [CrossRef]
20. Kwak, S.W.; Hong, J.H.; Lee, S.H.; Kim, M.; Chung, Y.; Lee, K.M.; Kim, Y.; Park, M.H. Synthesis and Photophysical Properties of a Series of Dimeric Indium Quinolinates. *Molecules* **2021**, *26*, 34. [CrossRef]
21. Qi, Y.; Kang, R.; Huang, J.; Zhang, W.; He, G.; Yin, S.; Fang, Y. Reunderstanding the Fluorescent Behavior of Four-Coordinate Monoboron Complexes Containing Monoanionic Bidentate Ligands. *J. Phys. Chem. B* **2017**, *121*, 6189–6199. [CrossRef]
22. Bakewell, C.; White, A.J.P.; Long, N.J.; Williams, C.K. 8-Quinolinolato Gallium Complexes: Iso-selective Initiators for *rac*-Lactide Polymerization. *Inorg. Chem.* **2013**, *52*, 12561–12567. [CrossRef] [PubMed]
23. Hellstrom, S.L.; Ugolotti, J.; Britovsek, G.J.P.; Jones, T.S.; White, A.J.P. The effect of fluorination on the luminescent behaviour of 8-hydroxyquinoline boron compounds. *New J. Chem.* **2008**, *32*, 1379–1387. [CrossRef]
24. Qin, Y.; Pagba, C.; Piotrowiak, P.; Jäkle, F. Luminescent Organoboron Quinolate Polymers. *J. Am. Chem. Soc.* **2004**, *126*, 7015–7018. [CrossRef] [PubMed]
25. Wrackmeyer, B. Organoboranes and tetraorganoborates studied by ^{11}B and ^{13}C NMR spectroscopy and DFT calculations. *Z. Naturforsch. B* **2015**, *70*, 421–424. [CrossRef]
26. Zhang, N.; Wang, C.; Zou, G.; Tang, J. Palladium-catalyzed cross-coupling of aryl chlorides with O, N-chelate stabilized diarylborinates. *J. Organomet. Chem.* **2017**, *842*, 54–58. [CrossRef]
27. Yamaguchi, I.; Iijima, T.; Yamamoto, T. Synthesis and reactivity of Al(Et)q′$_2$ (q′=2-methyl-8-quinolinolato) and crystal structures of [Al(Et)$_2$q]$_2$ and Alq′$_2$q (q=8-quinolinolato). *J. Organomet. Chem.* **2002**, *654*, 229–232. [CrossRef]
28. Pan, J.; Kampf, J.W.; Ashe, A.J. Tricarbonylchromium Complexes of 1,2-Dihydro-1,2-benzazaborines. *Organometallics* **2009**, *28*, 506–511. [CrossRef]
29. Wu, Q.; Esteghamatian, M.; Hu, N.-X.; Popovic, Z.; Enright, G.; Tao, Y.; D'Iorio, M.; Wang, S. Synthesis, Structure, and Electroluminescence of BR$_2$q (R = Et, Ph, 2-Naphthyl and q = 8-Hydroxyquinolato). *Chem. Mater.* **2000**, *12*, 79–83. [CrossRef]
30. Höpfl, H.; Barba, V.; Vargas, G.; Farfan, N.; Santillan, R.; Castillo, D. X-ray crystallographic study of three (N→B)-borinates prepared from 8-hydroxyquinoline and 2-hydroxypyridine. *Chem. Heterocycl. Compd.* **1999**, *35*, 912–927. [CrossRef]
31. Hu, T.-C.; Wu, M.-C.; Wu, S.-S.; Hu, C.-H.; Lin, C.-H.; Datta, A.; Lin, T.-H.; Huang, J.-H. Synthesis, characterization and reactivity study of aluminum compounds incorporating bi- and tri-dentate pyrrole–piperazine ligands. *RSC Adv.* **2016**, *6*, 16331–16339. [CrossRef]
32. Francis, J.A.; Bott, S.G.; Barron, A.R. Aluminium compounds containing bidentate ligands: Chelate ring size and rigid conformation effects. *J. Chem. Soc. Dalton Trans.* **1998**, 3305–3310. [CrossRef]
33. Bulteau, Y.; Tarrat, N.; Pébère, N.; Lacaze-Dufaure, C. 8-Hydroxyquinoline complexes (Alq$_3$) on Al(111): Atomic scale structure, energetics and charge distribution. *New J. Chem.* **2020**, *44*, 15209–15222. [CrossRef]
34. Hohenberg, P.; Kohn, W. Inhomogeneous Electron Gas. *Phys. Rev. B* **1964**, *136*, 864–871. [CrossRef]
35. Kohn, W.; Sham, L.J. Self-consistent equations including exchange and correlation effects. *Phys. Rev. A* **1965**, *140*, 1133–1138. [CrossRef]
36. Yanai, T.; Tew, D.; Handy, N. A new hybrid exchange–correlation functional using the Coulomb-attenuating method (CAM-B3LYP). *Chem. Phys. Lett.* **2004**, *393*, 51–57. [CrossRef]

37. Dunning, T.H., Jr. Gaussian basis sets for use in correlated molecular calculations. I. The atoms boron through neon and hydrogen. *J. Chem. Phys.* **1989**, *90*, 1007–1023. [CrossRef]
38. Neese, F. The ORCA program system. *Wiley Interdiscip. Rev. Comput. Mol. Sci.* **2012**, *2*, 73–78. [CrossRef]
39. Frisch, M.J.; Trucks, G.W.; Schlegel, H.B.; Scuseria, G.E.; Robb, M.A.; Cheeseman, J.R.; Scalmani, G.; Barone, V.; Petersson, G.A.; Nakatsuji, H.; et al. *Gaussian 16 Rev. C.01*; Gaussian, Inc.: Wallingford, CT, USA, 2016.
40. Lu, T.; Chen, F. Multiwfn: A multifunctional wavefunction analyzer. *J. Comput. Chem.* **2012**, *33*, 580–592. [CrossRef]
41. Glendening, E.D.; Badenhoop, J.K.; Reed, A.E.; Carpenter, J.E.; Bohmann, J.A.; Morales, C.M.; Karafiloglou, P.; Landis, C.R.; Weinhold, F. *NBO 7.0*; Theoretical Chemistry Institute, University of Wisconsin: Madison, WI, USA, 2018.
42. Barone, V.; Cossi, M. Quantum Calculation of Molecular Energies and Energy Gradients in Solution by a Conductor Solvent Model. *J. Phys. Chem. A* **1998**, *102*, 1995–2001. [CrossRef]
43. Vogler, A.; Kunkely, H. Luminescent Metal Complexes: Diversity of Excited States. In *Transition Metal and Rare Earth Compounds: Excited States, Transitions, Interactions*; Yersin, H.I., Ed.; Springer: Berlin/Heidelberg, Germany, 2001; pp. 143–182.
44. Burrows, H.D.; Fernandes, M.; Seixas de Melo, J.; Monkman, A.P.; Navaratnam, S. Characterization of the Triplet State of Tris(8-hydroxyquinoline)aluminium(III) in Benzene Solution. *J. Am. Chem. Soc.* **2003**, *125*, 15310–15311. [CrossRef] [PubMed]
45. Martin, R.L. Natural transition orbitals. *J. Chem. Phys.* **2003**, *118*, 4775–4777. [CrossRef]
46. Humphrey, W.; Dalke, A.; Schulten, K. VMD: Visual molecular dynamics. *J. Mol. Graph.* **1996**, *14*, 33–38. [CrossRef]
47. Pérez-Bolívar, C.; Montes, V.A.; Anzenbacher, P. True Blue: Blue-Emitting Aluminum(III) Quinolinolate Complexes. *Inorg. Chem.* **2006**, *45*, 9610–9612. [CrossRef]
48. Dolomanov, O.V.; Bourhis, L.J.; Gildea, R.J.; Howard, J.A.K.; Puschmann, H. OLEX2: A complete structure solution, refinement and analysis program. *J. Appl. Cryst.* **2009**, *42*, 339–341. [CrossRef]
49. Sheldrick, G.M. *SHELXT*—Integrated space-group and crystal-structure determination. *Acta Crystallogr. Sect. A Found. Adv.* **2015**, *71*, 3–8. [CrossRef]
50. Sheldrick, G.M. Crystal structure refinement with *SHELXL*. *Acta Crystallogr. Sect. C Struct. Chem.* **2015**, *71*, 3–8. [CrossRef]
51. Mohammadnezhad, G.; Amini, M.M.; Khavasi, H.R.; Plass, W. Structural and spectroscopic characterizations of aluminum phenoxide. *Spectrochim. Acta A* **2016**, *157*, 238–243. [CrossRef]